C–H Activation

Deutsche Ausgabe: DOI: 10.1002/ange.201511507
Internationale Ausgabe: DOI: 10.1002/anie.201511507

Activation of Methane and Ethane as Mediated by the Triatomic Anion $HNbN^-$: Electronic Structure Similarity with a Pt Atom

Jia-Bi Ma, Lin-Lin Xu, Qing-Yu Liu, and Sheng-Gui He**

Abstract: *Investigations of the intrinsic properties of gas-phase transition metal nitride (TMN) ions represent one approach to gain a fundamental understanding of the active sites of TMN catalysts, the activities and electronic structures of which are known to be comparable to those of noble metal catalysts. Herein, we investigate the structures and reactivities of the triatomic anions $HNbN^-$ by means of mass spectrometry and photoelectron imaging spectroscopy, in conjunction with density functional theory calculations. The $HNbN^-$ anions are capable of activating CH_4 and C_2H_6 through oxidative addition, exhibiting similar reactivities to free Pt atoms. The similar electronic structures of $HNbN^-$ and Pt, especially the active orbitals, are responsible for this resemblance. Compared to the inert NbN^-, the coordination of the H atom in $HNbN^-$ is indispensable. New insights into how to replace noble metals with TMNs may be derived from this combined experimental/computational study.*

Since the pioneering work of Volpe and Boudart,[1] who developed a way to prepare Mo_2N powders with a high surface area, transition metal nitrides (TMNs) are often applied as heterogeneous catalysts in hydroprocessing and numerous other reactions.[2] Because the activities of TMNs resemble those of noble metals (NMs), such as Pt, they are reported as one of most promising replacements for costly NMs. Minimizing the use of NM catalysts and maximizing atom utilization while retaining the desired catalytic activities have been the focus of significant research topic for a long time. To achieve this goal, the establishment of structure–property relationships, the characterization of the active sites, and detailed knowledge about the reaction mechanisms are required. However, it is still quite challenging to obtain this insight directly and clearly from "real-life" experiments. A useful approach to investigate important details of related condensed-phase reactions takes advantage of state-of-the-art gas-phase experiments in conjunction with computational studies.[3]

Alkane, especially methane, C–H bonds are chemically very inert. Platinum ($5d^96s^1$)-related condensed-phase catalysts[4] and gas-phase clusters[5] show high reactivity in the context of thermal methane activation. As the simplest Pt-related systems, atomic species, Pt^+ and Pt^- ions, and Pt atoms, exhibit different reactivities toward CH_4.[5a,d,f,j] It is known that Pt^+ and Pt are reactive with CH_4, while Pt^- is not reactive. Understanding the electronic level similarity between Pt^q ($q = 0, \pm 1$) and TMN systems serves as the first step to interpret how to replace NMs by TMNs. It is also noteworthy that, in reactions with alkanes, anions are usually much less reactive than their cationic counterparts.[6] A literature survey shows that very few NM free anions can activate the C–H bond of methane, namely $(La_2O_3)_{3,4}O^-$,[6b] $Fe(CO)_2^-$,[7] and FeC_6^-.[8]

In gas-phase studies, little attention has been paid to the reactivities of NM-free nitride ions toward alkanes. Recently, Schwarz et al. reported the thermal reaction of the amido-nickel cation, $Ni(NH_2)^+$, with C_2H_4,[9] and Bernstein and co-workers investigated the reactivity of Co_xN_y toward H_2.[10] Herein, we report the smallest nitride anions $HNbN^-$, which activates CH_4 and C_2H_6 at room temperature.

The $HNbN^-$ anions were generated, mass-selected, confined and cooled, and then interacted with CH_4 and C_2H_6 in a linear ion trap (LIT) reactor. As shown in Figure 1a, in addition to $HNbN^-$, a weak signal of $HNbNO^-$ was generated, which can be produced from the reaction of $HNbN^-$ with water impurities in the LIT, according to: $HNbN^- + H_2O \rightarrow HNbNO^- + H_2$. Upon reacting with CH_4 at 1.19 Pa for about 7 ms (Figure 1b), the adsorption product $HNbNCH_4^-$ was observed (Reaction 1); a weak signal corresponding to $HNbN(CH_4)_2^-$ also shows up due to secondary reactions.

$$HNbN^- + CH_4 \rightarrow HNbNCH_4^- \quad (1)$$

When C_2H_6 at a pressure of 0.77 Pa was introduced and interacted with $HNbN^-$ for 2 ms (Figure 1d), two new signals were generated, indicating that ethene and H_2 molecules are produced and liberated:

$$HNbN^- + C_2H_6 \rightarrow H_3NbN^- + C_2H_4 \quad 16\% \quad (2a)$$

$$HNbN^- + C_2H_6 \rightarrow HNbNC_2H_4^- + H_2 \quad 84\% \quad (2b)$$

These reactions were confirmed by performing isotopic labelling experiments with CD_4 and CH_3CD_3 (Figure 1c and e, respectively). Notably, NbN^- anions were inert toward

[*] Dr. J.-B. Ma, L.-L. Xu
The Institute for Chemical Physics
Key Laboratory of Cluster Science
School of Chemistry, Beijing Institute of Technology
Beijing, 100081 (China)
E-mail: majiabi@bit.edu.cn
Q.-Y. Liu, Prof. Dr. S.-G. He
Beijing National laboratory for Moulecular Science
State Key Laboratory for Structural Chemistry of Unstable and Stable Species
Institute of Chemistry, Chinese Academy of Sciences
100190, Beijing (China)
E-mail: shengguihe@iccas.ac.cn

Supporting information for this article can be found under: http://dx.doi.org/10.1002/anie.201511507.

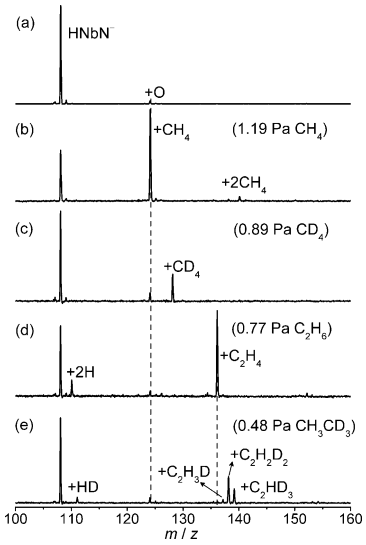

Figure 1. Time-of flight mass spectra for the reactions of mass-selected $HNbN^-$ (a), with CH_4 (b), CD_4 (c) for 7 ms, and with C_2H_6 (d) and CH_3CD_3 (e) for 2 ms. The effective reactant gas pressures are shown. The label +X denotes $HNbNX^-$ (X = CH_4, C_2H_4).

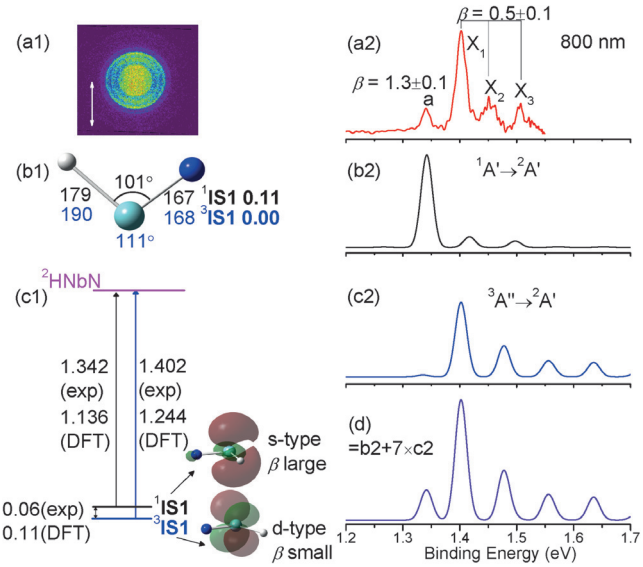

Figure 2. a1) Photoelectron image and a2) photoelectron spectrum of $HNbN^-$ at laser wavelength of 800 nm (see Figure S4). An arrow in a1 indicates the polarization of the laser. b1) The DFT calculated structures of ^{1}**IS1** (black) as well as ^{3}**IS1** (blue), respectively. Bond lengths and angles (∡N-Nb-H) are in pm and degrees, respectively. c1) Diagram showing electronic transitions between ^{1}**IS1**/^{3}**IS1** and corresponding neutral species ^{2}HNbN (see Figure S4g). b2 and c2) Franck–Condon simulations of the transitions for ^{1}**IS1** and ^{3}**IS1**, respectively. The peaks in panels b2 and c2 are blue shifted by 0.206 and 0.158 eV, respectively, compared to the a and X bands in panel a2. d) The simulated photoelectron spectrum. The simulated coefficients were obtained by fitting the peak ratio of a:X in panel a2. The unshifted spectra are shown in Figure S4d–4f.

alkanes (Supporting Information, Figure S1). The pseudo-first-order rate constants (k_1) of Reactions 1 and 2 were estimated to be 5.3×10^{-13} cm^3 molecule^{-1} s^{-1} and 2.7×10^{-12} cm^3 molecule^{-1} s^{-1}, corresponding to efficiencies (∅)[11] of 0.05 % and 0.3 %, respectively. The kinetic isotope effects (KIEs), defined as $k_1(HNbN^- + CH_4)/k_1(HNbN^- + CD_4)$ and $k_1(HNbN^- + C_2H_6)/k_1(HNbN^- + CH_3CD_3)$, amounted to 2.0 and 1.2, respectively. The signal dependence of product ions on CH_4, CD_4, C_2H_6, and CH_3CD_3 pressures were derived and fitted with the experimental data (Figure S2). The single-exponential decays of the $HNbN^-$ intensities with respect to the alkane pressures imply that most (> 85 %) of the generated $HNbN^-$ anions have a uniform structure.

Density functional theory (DFT) calculations were performed to study the structures of $HNbN^-$, and two isomers were determined for this triatomic anion. As predicted by BMK,[12] which was the one of the few functionals giving good results among the 20 tested methods (Table S1),[13] a bent structure with a triplet spin multiplicity (^{3}**IS1**, 3A″) is 0.11 eV more stable than its singlet electromer ^{1}**IS1** (1A′), and linear structures are higher (> 0.3 eV) in energy (**IS2**; Figure S3a). Photoelectron imaging (PEI) spectroscopy is an important and powerful technique to probe electronic structures, and a wealth of unambiguous information can be provided. The experimental and simulated PEI spectra of $HNbN^-$ are shown in Figure 2. The values of the anisotropy parameter β,[14] indicate that the first band ($\beta = 1.3\pm0.1$) and the other three bands ($\beta = 0.5\pm0.1$) correspond to the electron detachments from two different types of atomic orbitals; thus, two different electronic transitions should be involved (Figure 2a2). In addition, the a band corresponds to an adiabatic detachment energy (ADE) of 1.342 eV, and the X_1 band is located at a slightly higher binding energy (ADE = 1.402 eV). The simulated PEI spectra (Figure 2b2-d), based on **IS1** with multiplicities 1 and 3 (Figure 2b1), suggest that there are two isomers present in the ion source: the low binding energy feature (a band) comes from excitation of the Nb 5s-type orbital in ^{1}**IS1**, and the features above 1.40 eV (bands X_1-X_3) correspond to detachment from a Nb 4d-type orbital in ^{3}**IS1** (Figure 2c1). When these two simulated spectra are combined by a suitable ratio (1:7), the spectrum shown in Figure 2d fits well with the experimental spectrum given in Figure 2a2. In conclusion, the ground state of $HNbN^-$ corresponds to a high-spin state ^{3}**IS1** and the low-spin ^{1}**IS1** forms the excited state. The energy of ^{3}**IS1** is 0.06 eV lower than that of ^{1}**IS1**, indicating that the BMK-calculated triplet–singlet energy gap is overestimated by 0.05 eV relative to the experimental data. Natural bond orbital analysis demonstrated that in ^{1}**IS1** and ^{3}**IS1**, the Nb–N and Nb–H bond orders amount to ≈3 and ≈1, respectively, and the triplet-bond character of the Nb–N bond in $HNbN^-$ is similar to those of terminal metal nitrides (M≡N) in transition metal complexes.[15]

In this context, it is quite interesting and necessary to distinguish which spin state, ^{1}**IS1** or ^{3}**IS1**, acts as the active species. Surprisingly, the open-shell species ^{3}**IS1** is not capable of activating alkanes owing to substantial barriers (panels a and b in Figure S5). In contrast, the closed-shell species ^{1}**IS1** reacts, at least according to the DFT calculations. The lowest energy reaction pathways for Reactions 1 and 2 are shown in Figures 3 and S6, respectively (see Figures S7–S10 for alternatives considered). The electrostatic potential (Figure S3b) indicates that the CH_4 molecule prefers to be weakly

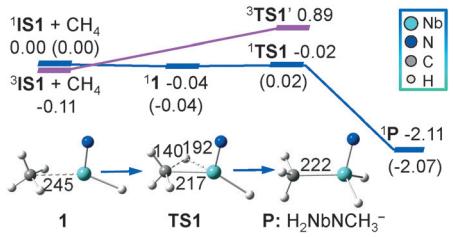

Figure 3. DFT-calculated potential energy surface (PES) for the reaction of $HNbN^-$ with CH_4. Selected bond lengths are given in pm. The zero-point vibration corrected energies (ΔH_{0K} in eV) of the reaction intermediates, transition states, and products with respect to the separated reactants are given. The relative ΔH_{0K} energies for the reaction with CD_4 are given in brackets. All structures given refer to the singlet surface. The superscripts indicate the spin states of species.

adsorbed over the Nb-side because it is less negatively charged than the other sides of the anion. As shown in Figure 3, C–H bond activation of CH_4 by the niobium atom proceeds through oxidative addition (OA), leading to the formation of an oxidative adsorption complex of $H_2NbNCH_3^-$ (**P**), and in a rather exothermic process (−2.11 eV, with respect to the separated reactants). The bond orders of Nb–N and Nb–H in $HNbN^-$ are almost unchanged during the process. Both the dissociation rate (k_d) of $^1\mathbf{1}\rightarrow{}^1\mathbf{IS1} + CH_4$ ($> 2.1\times10^{11}$ s^{-1}, the lower limit of k_d) and the rate constant of $^1\mathbf{1}\rightarrow{}^1\mathbf{TS1}\rightarrow{}^1\mathbf{P}$ (about 3.6×10^{11} s^{-1}) are much larger than the collision rate of $^1\mathbf{1}$ with the cooling gas He ($k_{collision}\approx 1.1\times10^6$ s^{-1}; see the Supporting Information for details), suggesting $^1\mathbf{1}$ is not stable. In addition, the C–H bond activation product H_2 is liberated when higher center-of-mass collisional energy ($\approx$0.3 eV) is added to the $HNbN^-/CH_4$ system under single-collision conditions (Figure S11). Thus, the observed $HNbNCH_4^-$ in Figure 1 is the dissociative adsorption product. A small overall positive barrier (0.02 eV, Figure 3) is involved in the reaction with CD_4, and its rate constant $k_1(HNbN^- + CD_4)$ is 2.6×10^{-13} cm^3 molecule^{-1} s^{-1}. For the reactions of transition metal cations, such as Ir^+, with CH_4, H_2 elimination is also observed.[3b] However, DFT calculations predict that this channel is not favorable in the thermal reaction of $HNbN^-$ with CH_4 (Figure S12), which is in line with the mass spectrometry data (Figure 1b and c). As shown in Figure S6, an OA/reductive elimination mechanism is operative for the $HNbN^-/C_2H_6$ system, and the DFT results are in good agreement with the MS results. For a detailed description of the pathways, see the Supporting Information. As mentioned above, the ground state $^3\mathbf{IS1}$ is inert toward alkanes; however, most of the generated $HNbN^-$ anions do react with alkanes. Consequently, a two-state reactivity (TSR) scenario[16] is expected to prevail. As predicted by DFT calculations, the crossing point (CP) occurs along $^3\mathbf{IS1} + CH_4\rightarrow{}^1\mathbf{IS1}$ (Figure S13b), indicating that the facile spin flip triplet→singlet takes place at the entrance channel when methane approaches to $HNbN^-$. In doing so, the prohibitively high-energy triplet barrier is bypassed. The scenario of a TSR pattern holds true also for the $HNbN^-/C_2H_6$ (Figure S14) similar to that of $HNbN^-/CH_4$. The spin flip can be responsible for the low reaction efficiencies of Reactions 1 (0.05%) and 2 (0.3%). Although the spin flips could happen from a thermodynamic point of view, the efficiencies are unknown.

It is noteable that NbN^- does not react with alkanes (Figure S1). Although the hydrogen atom of $HNbN^-$ is not directly involved in the reaction processes and thus seems like a spectator ligand, its very presence is crucial to achieve the activation of alkanes. To investigate the special role of the H ligand, DFT calculations were carried out on reactions of Nb^- and NbN^- with CH_4 and C_2H_6 (Figures S15 and S16, respectively). In NbN^-, the Nb–N bond length is 169 pm[17] and the bond order corresponds to 3.5. One additional H atom forms a covalent bond with the niobium atom, and the Nb–H bond formation involves one electron from the hydrogen 1s orbital and one from an sd hybrid on the Nb atom. The coordination with open-shell ligands, for example, N and H atoms, helps to stabilize the low-spin states of $HNbN^-$ species and to render the Nb-side less negatively charged. Both of these features are favorable factors for C–H bond of activation alkanes by OA. Such a ligand effect crucially affects the reactivity of bond activation processes.[18]

If TMN species function as viable substitutes of NM atoms, Pt for instance, their chemistry should be similar. To achieve this goal, designing gas-phase TMN species, with similar electronic structure to Pt,[3e,19] is one promising way. $HNbN^-$ has the valence electron count (VEC) of 12, but due to the formation of one Nb–H bond, its effective VEC is reduced to 10, which is the same value as that of Pt. A more careful comparison between methane (and ethane) activation over $HNbN^-$ and Pt atom reveals other similarities in both electronic structures and reactivities. From an electronic structural point of view, the ground states of both $HNbN^-$ and Pt atom are triplet, and singlet states lie 0.06 eV and 0.76 eV[20] above the ground states, respectively. Moreover, $HNbN^-$ and Pt[5f,j] can bring about insertion into C–H bond of CH_4. Elimination of H_2 and C_2H_4, observed in the $HNbN^-/C_2H_6$ system, also exists in the reaction of Pt with C_2H_6, as predicted theoretically.[5i] The similar reactivities of singlet $HNbN^-$ ($^1\mathbf{IS1}$) and singlet Pt atom can be attributed to the similar nature of their highest occupied molecular orbitals (HOMOs). The highest five orbitals of ^{1}Pt atom are degenerate (Figure 4). The OA of the C–H bond in CH_4 mediated

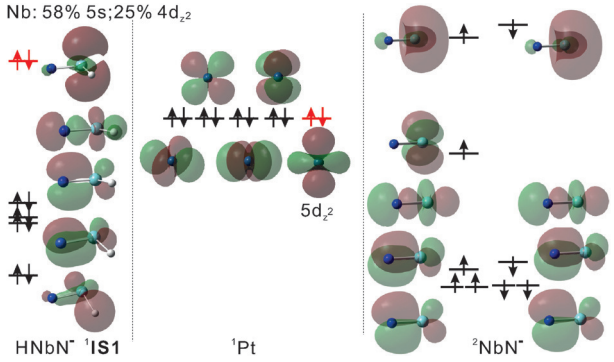

Figure 4. Parts of electronic structures of the singlet $HNbN^-$ ($^1\mathbf{IS1}$), the singlet Pt atom, and the doublet NbN^-. The superscripts indicate the spin states of species.

by ^{1}Pt atom is barrierless.[5a,e,j] The orbital analysis along the relaxed potential energy curve formed by decreasing the distance between the C and H atom in the singlet $HPtCH_3$ insertion intermediate indicates that the Pt d_{z^2} orbital is the essential one for the reaction; 5d/6s hybridization may also happen (Figure S17). It is known that the relativistic effect influences the ordering of the 5d and 6s orbitals of Pt with respect to each other, thus favoring 5d/6s hybridization and formation of new bonds with reactant molecules.[21] For $HNbN^-$, the HOMO is mainly composed of the Nb 5s (58%) and $4d_{z^2}$ (25%), that is the 4d/5s hybrid orbital, and exhibits the similar shape with d_{z^2} orbital (Figure 4). In the PEI experiments of $HNbN^-$, the nature of the 5s orbital of the Nb atom dominates, corresponding to the a band with large β in Figure 2a2, while d_{z^2} has the primary contribution to the CH_4 activation reaction, reflected by the composition analysis of the HOMO of **TS1**. As shown in Figure S17, Nb $4d_{z^2}$ (42%) is the main composition in the HOMO of **TS1**. In sharp contrast, in the NbN^-/CH_4 system, the HOMO of **TS10** is with high percentage (62%) of Nb 5s orbital rather than $4d_{z^2}$, and this pathway is kinetically restricted. When compared with the inert NbN^- and the reactive $HNbN^-$, we can draw the conclusion that by forming the Nb–H bond in $HNbN^-$, the active 4d/5s hybrid orbital of the Nb atom is formed. Therefore, designing TMN species having similar electronic structures to NMs, especially similar active orbitals, may contribute one important way to replace NMs with TMNs; coordination of H atoms (or other open-shell ligands) sometimes is indispensable to achieve this goal.

In conclusion, the triatomic anion $HNbN^-$ corresponds to a noble-metal free system, and to the best of our knowledge, this is among the first to report alkane activation by transition metal nitride ions. Synthesizing transition metal nitrides with similar electronic structures, especially active orbitals, to noble metals coupled with the regulation of open-shell ligands, such as H atoms, may be one valid way to tailor the design of new and cheap catalysts through partial or full substitution of noble metals.

Acknowledgements

We particularly appreciate Professor Helmut Schwarz and Professor Ricardo B. Metz for valuable discussions and insightful comments. This work is supported by the National Natural Science Foundation of China (Nos. 21503015 and 21273247).

Keywords: density functional theory · mass spectrometry · methane activation · nitrides · photoelectron spectroscopy

How to cite: *Angew. Chem. Int. Ed.* **2016**, *55*, 4947–4951
Angew. Chem. **2016**, *128*, 5031–5035

[1] L. Volpe, M. Boudart, *J. Solid State Chem.* **1985**, *59*, 332–347.
[2] a) E. Furimsky, *Appl. Catal. A* **2003**, *240*, 1–28; b) W. T. Yao, P. Makowski, C. Giordano, F. Goettmann, *Chem. Eur. J.* **2009**, *15*, 11999–12004; c) A. M. Alexander, J. S. J. Hargreaves, *Chem. Soc. Rev.* **2010**, *39*, 4388–4401; d) J. S. J. Hargreaves, *Coord. Chem. Rev.* **2013**, *257*, 2015–2031.
[3] a) R. A. J. O'Hair, G. N. Khairallah, *J. Cluster Sci.* **2004**, *15*, 331–363; b) F.-X. Li, X.-G. Zhang, P. B. Armentrout, *Int. J. Mass Spectrom.* **2006**, *255*, 279–300; c) J. Roithová, D. Schröder, *Chem. Rev.* **2010**, *110*, 1170–1211; d) H. Schwarz, *Angew. Chem. Int. Ed.* **2011**, *50*, 10096–10115; *Angew. Chem.* **2011**, *123*, 10276–10297; e) A. W. Castleman, Jr., *Catal. Lett.* **2011**, *141*, 1243–1253; f) S. Yin, E. R. Bernstein, *Int. J. Mass Spectrom.* **2012**, *321–322*, 49–65; g) S. M. Lang, T. M. Bernhardt, *Phys. Chem. Chem. Phys.* **2012**, *14*, 9255–9269; h) E. Janssens, S. M. Lang, M. Brummer, A. Niedziela, G. Santambrogio, K. R. Asmis, J. Sauer, *Phys. Chem. Chem. Phys.* **2012**, *14*, 14344–14353; i) H. Yamamoto, K. Miyajima, T. Yasuike, F. Mafune, *J. Phys. Chem. A* **2013**, *117*, 12175–12183; j) H. Schwarz, *Isr. J. Chem.* **2014**, *54*, 1413–1431; k) Q.-Y. Liu, S.-G. He, *Chem. J. Chin. U.* **2014**, *35*, 665–688.
[4] a) R. A. Periana, D. J. Taube, S. Gamble, H. Taube, T. Satoh, H. Fujii, *Science* **1998**, *280*, 560–564; b) W. Tang, Z. P. Hu, M. J. Wang, G. D. Stucky, H. Metiu, E. W. McFarland, *J. Catal.* **2010**, *273*, 125–137; c) O. A. Mironov, S. M. Bischof, M. M. Konnick, B. G. Hashiguchi, V. R. Ziatdinov, W. A. Goddard, M. Ahlquist, R. A. Periana, *J. Am. Chem. Soc.* **2013**, *135*, 14644–14658.
[5] a) J. J. Carroll, J. C. Weisshaar, P. E. M. Siegbahn, C. A. M. Wittborn, M. R. A. Blomberg, *J. Phys. Chem.* **1995**, *99*, 14388–14396; b) U. Achatz, C. Berg, S. Joos, B. S. Fox, M. K. Beyer, G. Niedner-Schatteburg, V. E. Bondybey, *Chem. Phys. Lett.* **2000**, *320*, 53–58; c) D. Schröder, H. Schwarz, *Can. J. Chem.* **2005**, *83*, 1936–1940; d) C. Adlhart, E. Uggerud, *Chem. Commun.* **2006**, 2581–2582; e) L. Xiao, L.-C. Wang, *J. Phys. Chem. B* **2007**, *111*, 1657–1663; f) H. G. Cho, L. Andrews, *Organometallics* **2009**, *28*, 1358–1368; g) D. J. Harding, C. Kerpal, G. Meijer, A. Fielicke, *Angew. Chem. Int. Ed.* **2012**, *51*, 817–819; *Angew. Chem.* **2012**, *124*, 842–845; h) S.-L. Liu, Z.-Y. Geng, Y.-C. Wang, Y.-F. Yan, *J. Phys. Chem. A* **2012**, *116*, 4560–4568; i) F.-M. Li, H.-Q. Yang, T.-Y. Ju, X.-Y. Li, C.-W. Hu, *Comput. Theor. Chem.* **2012**, *994*, 112–120; j) M. Perera, R. B. Metz, O. Kostko, M. Ahmed, *Angew. Chem. Int. Ed.* **2013**, *52*, 888–891; *Angew. Chem.* **2013**, *125*, 922–925; k) D. J. Harding, A. Fielicke, *Chem. Eur. J.* **2014**, *20*, 3258–3267; l) Y.-X. Zhao, Z.-Y. Li, Z. Yuan, X.-N. Li, S.-G. He, *Angew. Chem. Int. Ed.* **2014**, *53*, 9482–9486; *Angew. Chem.* **2014**, *126*, 9636–9640.
[6] a) G. E. Johnson, R. Mitrić, M. Nossler, E. C. Tyo, V. Bonačić-Koutecký, A. W. Castleman, Jr., *J. Am. Chem. Soc.* **2009**, *131*, 5460–5470; b) J.-H. Meng, X.-J. Deng, Z.-Y. Li, S.-G. He, W.-J. Zheng, *Chem. Eur. J.* **2014**, *20*, 5580–5583.
[7] R. N. Mcdonald, D. J. Reed, A. K. Chowdhury, *Organometallics* **1989**, *8*, 1122–1124.
[8] H.-F. Li, Z.-Y. Li, Q.-Y. Liu, X.-N. Li, Y.-X. Zhao, S.-G. He, *J. Phys. Chem. Lett.* **2015**, *6*, 2287–2291.
[9] R. Kretschmer, M. Schlangen, H. Schwarz, *Angew. Chem. Int. Ed.* **2012**, *51*, 3483–3488; *Angew. Chem.* **2012**, *124*, 3541–3546.
[10] S. Yin, Y. Xie, E. R. Bernstein, *J. Chem. Phys.* **2012**, *137*, 124304.
[11] a) G. Gioumousis, D. P. Stevenson, *J. Chem. Phys.* **1958**, *29*, 294–299; b) G. Kummerlöwe, M. K. Beyer, *Int. J. Mass Spectrom.* **2005**, *244*, 84–90.
[12] A. D. Boese, J. M. L. Martin, *J. Chem. Phys.* **2004**, *121*, 3405–3416.
[13] The BMK method gives the best interpretation of the PEI spectrum, and good prediction of Nb^+–H, Nb^+–CH_2, H–C_2H_5, and N–H bonds.
[14] a) D. M. Neumark, *J. Phys. Chem. A* **2008**, *112*, 13287–13301; b) Q.-Y. Liu, L.-R. Hu, Z.-Y. Li, C.-G. Ning, J.-B. Ma, H. Chen, S.-G. He, *J. Chem. Phys.* **2015**, *142*, 164301.
[15] J. M. Smith in *Progress in Inorganic Chemistry*, *Vol. 58* (Ed.: K. D. Karlin), Wiley, Hoboken, **2014**.
[16] D. Schröder, S. Shaik, H. Schwarz, *Acc. Chem. Res.* **2000**, *33*, 139–145.

[17] C. Berkdemir, S. B. Cheng, A. W. Castleman, Jr., *Int. J. Mass Spectrom.* **2014**, *365*, 222 – 224.
[18] R. Kretschmer, M. Schlangen, H. Schwarz, *Angew. Chem. Int. Ed.* **2013**, *52*, 6097 – 6101; *Angew. Chem.* **2013**, *125*, 6213 – 6217.
[19] S. J. Peppernick, K. D. D. Gunaratne, A. W. Castleman, Jr., *Proc. Natl. Acad. Sci. USA* **2010**, *107*, 975 – 980.
[20] C. E. Moore, *Atomic Energy Levels as Derived from the Analysis of Optical Spectra—Molybdenum through Lanthanum and Hafnium through Actinium*, *Vol. III*, Nat. Stand. Ref. Data Ser., Nat. Bur. Stand., **1958**.
[21] a) C. Heinemann, H. Schwarz, W. Koch, K. G. Dyall, *J. Chem. Phys.* **1996**, *104*, 4642 – 4651; b) P. Pyykkö, *Annu. Rev. Phys. Chem.* **2012**, *63*, 45 – 64.

Received: December 11, 2015
Revised: February 15, 2016
Published online: March 8, 2016

